PHYSICAL REVIEW D **85,** 024038 (2012)

Constraint damping for the Z4c formulation of general relativity

Andreas Weyhausen, Sebastiano Bernuzzi, and David Hilditch
Theoretical Physics Institute, University of Jena, 07743 Jena, Germany
(Received 28 July 2011; published 24 January 2012)

One possibility for avoiding constraint violation in numerical relativity simulations adopting free-evolution schemes is to modify the continuum evolution equations so that constraint violations are damped away. Gundlach *et al.* demonstrated that such a scheme damps low-amplitude, high-frequency constraint-violating modes exponentially for the Z4 formulation of general relativity. Here we analyze the effect of the damping scheme in numerical applications on a conformal decomposition of Z4. After reproducing the theoretically predicted damping rates of constraint violations in the linear regime, we explore numerical solutions not covered by the theoretical analysis. In particular we examine the effect of the damping scheme on low-frequency and on high-amplitude perturbations of flat spacetime as well and on the long-term dynamics of puncture and compact star initial data in the context of spherical symmetry. We find that the damping scheme is effective provided that the constraint violation is resolved on the numerical grid. On grid noise the combination of artificial dissipation and damping helps to suppress constraint violations. We find that care must be taken in choosing the damping parameter in simulations of puncture black holes. Otherwise the damping scheme can cause undesirable growth of the constraints, and even qualitatively incorrect evolutions. In the numerical evolution of a compact static star we find that the choice of the damping parameter is even more delicate, but may lead to a small decrease of constraint violation. For a large range of values it results in unphysical behavior.

DOI: 10.1103/PhysRevD.85.024038 PACS numbers: 04.25.D−, 04.30.Db, 95.30.Sf

I. INTRODUCTION

The most common way to construct numerical solutions to the field equations of general relativity is to take a free-evolution approach. The Hamiltonian and momentum constraints of the theory are explicitly solved only for initial data. Then the remaining field equations are rewritten in a suitable hyperbolic form, and the initial data can be evolved using the desired numerical method with this *hyperbolic formulation*. In the absence of boundaries the contracted Bianchi identities can be used to show that if the constraints are satisfied on one spacelike slice of a foliation, then they will be satisfied everywhere. However, numerical solutions violate the constraints. This violation can be considered under control if, when one applies more resolution to the problem, the constraint violation converges away at an appropriate rate. Nonetheless, even if the constraint violation converges away, at finite resolution constraint violation is undesirable. A number of strategies to minimize the violation have been considered. One is to choose the formulation such that every constraint propagates. In combination with suitable boundary conditions, the constraint violation on the numerical grid should then be propagated away. On the other hand, if the constraints do not propagate then any violation may sit on the grid and grow. Another strategy is to use a *constraint damping scheme*, namely, to modify the evolution equations so that the constraint-satisfying hypersurface becomes an attractor in phase space; such an evolution scheme is sometimes called a λ-system [1]. The constraints are then referred to as the λ-variables.

The Z4 formulation [2–7] has both propagating constraints and admits a constraint damping scheme [8]. The Z4 formulation has a close relationship with the generalized harmonic formulation, and the damping scheme is essentially the same for both systems. The damping scheme was a crucial ingredient in the first successful evolution of orbiting binary black holes through merger [9]. Analytic calculations demonstrating that constraint violations will be damped away are performed in the frozen coefficient approximation. On the basis of these calculations one expects that the damping scheme will be effective, in numerical applications, on constraint violations that are of low amplitude and high frequency in spacetimes that are close to stationarity. Since the constraint damping scheme is a modification of the continuum equations, this high frequency should be resolved on the numerical mesh. It is not clear what effect the damping scheme will have on ill-resolved numerical noise.

A conformal decomposition of Z4, called Z4c, was proposed [10,11] with the hope of bringing the advantages of propagating constraints and the constraint damping scheme to the puncture method [12,13] for the evolution of binary black holes. Here we continue that investigation, considering more carefully the effect of the constraint damping scheme on numerical evolutions. We address the following questions: (i) Under what conditions can the theoretically predicted damping rates be recovered in the numerical approximation? (ii) How effective is the damping scheme in astrophysically relevant spacetimes? (iii) In practical applications what are reasonable values for the constraint damping coefficients?

A variation of the conformal decomposition has been recently presented in [14]. There it was found that the constraint damping terms are essential for stable long-term 3D evolutions of binary black holes and the gauge wave test. Since the Z4c conformal decomposition differs from that in [14] by nonprincipal terms and implementation details (e.g. constraints projection and summation-by-part operators), our study does not necessarily apply in that case. More work is required to carefully evaluate the role of the constraint damping scheme in that case.

Because of the obvious computational overhead of working in three dimensions, we once again present numerical results in spherical symmetry. Note that since the constraint damping scheme is a modification to the continuum Z4c formulation, our results are expected to reflect the behavior of the full system. Working in spherical symmetry furthermore affords us the possibility of performing a thorough study in the parameter space of constraint damping coefficients.

In Sec. II we summarize the equations of motion for the Z4c formulation and describe the constraint damping scheme we employ. We also present the expected theoretical rates of damping in the high-frequency, frozen coefficient approximation. In Sec. III we present our numerical study. Finally we conclude in Sec. IV.

Notation. Geometric units are employed. Standard notation for the 3 + 1 general relativity is used, e.g. ∂_i, partial derivative with respect to coordinates x^i, $i = 1, 2, 3$, D_i, 3-covariant derivative, $\mathcal{L}_\beta$, Lie derivative along the vector β^i, γ, determinant of the 3-metric γ_{ij}, K_{ij}, α, β^i, extrinsic curvature, lapse function and shift vector. In the perturbed flat-space simulations there is no natural scale of time; there we give the time in abitrary units.

II. THE Z4C CONSTRAINT DAMPING SCHEME

A. The Z4c formulation

In 3 + 1 form the field equations of the Z4c formulation of general relativity for the three-metric and extrinsic curvature read

$$\partial_t \gamma_{ij} = -2\alpha K_{ij} + \mathcal{L}_\beta \gamma_{ij}, \tag{1}$$

$$\begin{aligned}\partial_t K_{ij} = &-D_i D_j \alpha + \alpha[R_{ij} - 2K_i{}^k K_{kj} + K K_{ij} \\ &+ 2\hat{D}_{(i} Z_{j)} - \kappa_1(1+\kappa_2)\gamma_{ij}\Theta] \\ &+ 4\pi\alpha[\gamma_{ij}(S - \rho_{\mathrm{ADM}}) - 2S_{ij}] + \mathcal{L}_\beta K_{ij},\end{aligned} \tag{2}$$

where we use the notation

$$\hat{D}_i Z_j \equiv \gamma^{-1/3}\gamma_{kj}\partial_i[\gamma^{1/3} Z^k]. \tag{3}$$

The constraints Θ, Z_i evolve according to

$$\partial_t \Theta = \alpha\left[\frac{1}{2}H + \hat{D}^i Z_i - \kappa_1(2+\kappa_2)\Theta\right] + \mathcal{L}_\beta \Theta, \tag{4}$$

$$\begin{aligned}\partial_t Z_i = &\alpha[M_i + D_i\Theta - \kappa_1 Z_i] \\ &+ \gamma^{1/3} Z^j \partial_t[\gamma^{-1/3}\gamma_{ij}] + \beta^j \hat{D}_j Z_i,\end{aligned} \tag{5}$$

where the Hamiltonian and momentum constraints H, M_i are given by

$$H = R - K_{ij}K^{ij} + K^2 - 16\pi\rho_{\mathrm{ADM}} = 0, \tag{6}$$

$$M_i = D^j[K_{ij} - \gamma_{ij}K] - 8\pi S_i = 0. \tag{7}$$

Their time dependence can be computed as (neglecting matter terms),

$$\begin{aligned}\partial_t H = &-2\alpha D^i M_i - 4M_i D^i\alpha + 2\alpha K H \\ &+ 2\alpha(2K\gamma^{ij} - K^{ij})\hat{D}_{(i} Z_{j)} \\ &- 4\kappa_1(1+\kappa_2)\alpha K\Theta + \mathcal{L}_\beta H,\end{aligned} \tag{8}$$

$$\begin{aligned}\partial_t M_i = &-\frac{1}{2}\alpha D_i H + \alpha K M_i - (D_i\alpha)H \\ &+ D^j(2\alpha\hat{D}_{(i} Z_{j)}) - D_i(2\alpha\gamma^{kl}\hat{D}_{(k} Z_{l)}) \\ &+ 2\kappa_1(1+\kappa_2)D_i(\alpha\Theta) + \mathcal{L}_\beta M_i.\end{aligned} \tag{9}$$

From Eq. (4) and (5) one sees that Θ, Z_i behave as λ variables if the free parameters $\kappa_{1,2}$ are properly chosen. Consequently the Einstein constraint are damped for $\kappa_1 > 0$ and $\kappa_2 > -1$ [8]. The constraint subsystem is closed. If the constraints Θ, Z_i and H, M_i are satisfied in one hypersurface they will remain satisfied at all times. Introducing the following variables and definitions,

$$\tilde{\gamma}_{ij} = \gamma^{-1/3}\gamma_{ij}, \qquad \chi = \gamma^{-1/3}, \tag{10}$$

$$\hat{K} = \gamma^{ij}K_{ij} - 2\Theta, \quad \tilde{A}_{ij} = \gamma^{-1/3}\left(K_{ij} - \frac{1}{3}\gamma_{ij}K\right), \tag{11}$$

$$\tilde{\Gamma}^i = 2\tilde{\gamma}^{ij} Z_j + \tilde{\gamma}^{ij}\tilde{\gamma}^{kl}\tilde{\gamma}_{jk,l}, \qquad \tilde{\Gamma}_{\mathrm{d}}{}^i = \tilde{\gamma}^{jk}\tilde{\Gamma}^i{}_{jk}, \tag{12}$$

the conformal evolutions equations, Z4c, read,

$$\partial_t \chi = \frac{2}{3}\chi[\alpha(\hat{K} + 2\Theta) - D_i\beta^i], \tag{13}$$

$$\partial_t \tilde{\gamma}_{ij} = -2\alpha\tilde{A}_{ij} + \beta^k\tilde{\gamma}_{ij,k} + 2\tilde{\gamma}_{k(i}\beta^k_{,j)} - \frac{2}{3}\tilde{\gamma}_{ij}\beta^k_{,k}, \tag{14}$$

$$\begin{aligned}\partial_t \hat{K} = &-D^i D_i\alpha + \alpha\left[\tilde{A}_{ij}\tilde{A}^{ij} + \frac{1}{3}(\hat{K} + 2\Theta)^2\right] \\ &+ 4\pi\alpha[S + \rho_{\mathrm{ADM}}] + \alpha\kappa_1(1-\kappa_2)\Theta + \beta^i\hat{K}_{,i}\end{aligned} \tag{15}$$

$$\begin{aligned}\partial_t \tilde{A}_{ij} = &\chi[-D_i D_j\alpha + \alpha(R_{ij} - 8\pi S_{ij})]^{\mathrm{tf}} \\ &+ \alpha[(\hat{K} + 2\Theta)\tilde{A}_{ij} - 2\tilde{A}^k{}_i\tilde{A}_{kj}] + \beta^k\tilde{A}_{ij,k} \\ &+ 2\tilde{A}_{k(i}\beta^k_{,j)} - \frac{2}{3}\tilde{A}_{ij}\beta^k{}_{,k}\end{aligned} \tag{16}$$

$$\partial_t \tilde{\Gamma}^i = -2\tilde{A}^{ij}\alpha_{,j} + 2\alpha\Big[\tilde{\Gamma}^i_{jk}\tilde{A}^{jk} - \frac{3}{2}\tilde{A}^{ij}\ln(\chi)_{,j} - \frac{1}{3}\tilde{\gamma}^{ij}(2\hat{K}+\Theta)_{,j} - 8\pi\tilde{\gamma}^{ij}S_j\Big] + \tilde{\gamma}^{jk}\beta^i_{,jk} + \frac{1}{3}\tilde{\gamma}^{ij}\beta^k_{,kj} + \beta^j\tilde{\Gamma}^i_{,j} - \tilde{\Gamma}_{\rm d}{}^j\beta^i_{,j} + \frac{2}{3}\tilde{\Gamma}_{\rm d}{}^i\beta^j_{,j} - 2\alpha\kappa_1(\tilde{\Gamma}^i - \tilde{\Gamma}_{\rm d}{}^i), \tag{17}$$

$$\partial_t\Theta = \alpha\Big[\frac{1}{2}R - \frac{1}{2}\tilde{A}_{ij}\tilde{A}^{ij} + \frac{1}{3}(\hat{K}+2\Theta)^2 - 8\pi\rho_{\rm ADM} - \kappa_1(2+\kappa_2)\Theta\Big] + \mathcal{L}_\beta\Theta. \tag{18}$$

Here the intrinsic curvature is written as

$$R_{ij} = R^\chi{}_{ij} + \tilde{R}_{ij}, \tag{19}$$

$$\tilde{R}^\chi{}_{ij} = \frac{1}{2\chi}\tilde{D}_i\tilde{D}_j\chi + \frac{1}{2\chi}\tilde{\gamma}_{ij}\tilde{D}^l\tilde{D}_l\chi - \frac{1}{4\chi^2}\tilde{D}_i\chi\tilde{D}_j\chi - \frac{3}{4\chi^2}\tilde{\gamma}_{ij}\tilde{D}^l\chi\tilde{D}_l\chi, \tag{20}$$

$$\tilde{R}_{ij} = -\frac{1}{2}\tilde{\gamma}^{lm}\tilde{\gamma}_{ij,lm} + \tilde{\gamma}_{k(i}\tilde{\Gamma}^k_{|,j)} + \tilde{\Gamma}_{\rm d}{}^k\tilde{\Gamma}_{(ij)k} + \tilde{\gamma}^{lm}(2\tilde{\Gamma}^k_{l(i}\tilde{\Gamma}_{j)km} + \tilde{\Gamma}^k_{im}\tilde{\Gamma}_{klj}). \tag{21}$$

The equations above are constrained by two algebraic expressions, $\ln(\det\tilde{\gamma}) = 0$ and $\tilde{\gamma}^{ij}\tilde{A}_{ij} = 0$, which are explicitly imposed during the numerical evolution. A solution of the evolution system is a solution of the Einstein system provided that Θ, Z_i, H and M_i vanish. In our numerical applications we close the system with the puncture gauge choice [15,16],

$$\partial_t\alpha = -\mu_L\alpha^2\hat{K} + \mathcal{L}_\beta\alpha, \tag{22}$$

$$\partial_t\beta^i = \mu_S\alpha^2\tilde{\Gamma}^i - \eta\beta^i + \beta^j\partial_j\beta^i, \tag{23}$$

with $\mu_L = 2/\alpha$, $\mu_S = 1/\alpha^2$ and $\eta = 2/M$, where M is the ADM mass of the spacetime. Unless stated otherwise, we employ the constraint-preserving boundary condition of [11].

For a more thorough introduction to the Z4c formulation we refer the reader to [10,11]. The full formulation generically forms a strongly hyperbolic system of partial differential equations, except in special cases which we do not discuss here.

B. Theoretical damping rates

Here we briefly review the results of [8], see also [17] for a discussion of stability of the undamped nonlinear constraint system. Consider the subsystem (4), (5), (8), and (9) when the initial data is constraint-violating. We consider a small constraint-violating perturbation on a background which satisfies the Z4c equations of motion. Working in the frozen coefficient approximation we can choose coordinates at a point so that the spatial metric is just that of flat space, and the lapse is unity. The only nontrivial component of the metric is the shift, which can only be made to vanish if we allow ourselves the freedom to change the spatial slice, which we take as given [18]. We discard nonprincipal terms involving products of the perturbation and the background curvature, extrinsic curvature, and matter sources, which is inconsistent with our first-order perturbation approach. The inclusion of matter sources without background curvature terms should give the correct damping rates for test matter fields on flat space. Such an analysis is not expected to give the rates for compact stars as evolved in Sec. III; nontrivial background curvature, extrinsic curvature and matter source terms will affect the damping rates, but for a consistent analysis all of these effects should be considered together. Already in the variable coefficient approximation such an analysis will be challenging. We will use the shift only to illustrate that it does not play any role on the damping rates. Besides the inclusion of the shift our calculations are exactly the same as those of [8]. To start with, we make a plane wave ansatz

$$\Theta = e^{st+i\omega_i x^i}\hat{\Theta}, \qquad Z_i = e^{st+i\omega_i x^i}\hat{Z}_i, \tag{24}$$

for the solution of the constraint subsystem, with complex s and real ω_i. We restrict to the special case $\kappa_2 = 0$, and write $\kappa_1 = k$. Rewriting the constraint subsystem in fully second order in time form, we find that following eigenvalue problem

$$\begin{pmatrix} \lambda + 2sk + 2i\omega\beta k & i\omega k \\ 0 & \lambda + sk - i\omega\beta k \end{pmatrix}\begin{pmatrix} \hat{\Theta} \\ \hat{Z}_{\hat{\omega}} \end{pmatrix} = 0, \tag{25}$$

$$(\lambda + sk - i\omega k\beta)(\hat{Z}_A) = 0, \tag{26}$$

must be satisfied, where we write

$$\lambda = s^2 + \omega^2 - 2i\omega s\beta - \omega^2\beta^2, \tag{27}$$

and $\hat{Z}_{\hat{\omega}}$ stands for the component of $\hat{Z}_i$ in the $\hat{\omega}^i$ direction, while $\hat{Z}_A$ are the components transverse to the unit wave vector $\hat{\omega}^i$ and $\beta = \beta^i\hat{\omega}_i$. The symbol of this equation generically has a complete set of eigenvectors, so the system can be rotated to diagonal form,

$$\begin{pmatrix} \lambda_\Theta & 0 \\ 0 & \lambda_{Z_{\hat{\omega}}} \end{pmatrix}\begin{pmatrix} s\hat{\Theta} + i\omega(\hat{Z}_{\hat{\omega}} - \beta\hat{\Theta}) \\ \hat{Z}_{\hat{\omega}} \end{pmatrix} = 0, \tag{28}$$

$$(\lambda_{Z_T})(\hat{Z}_A) = 0. \tag{29}$$

In one dimension, identifying the direction r, one expects that the behavior of the combinations of primitive variables,

$$u_\Theta = \partial_t \Theta + \partial_r Z_r, \tag{30}$$

$$u_\omega = Z_r \tag{31}$$

will be determined, in the linear regime, by the eigenvalues of the symbol provided that the shift is small. The eigenvalues are

$$\begin{aligned} \lambda_\Theta &= \lambda + 2sk - 2ik\omega\beta, \\ s &= -k + i\omega\beta \pm \sqrt{k^2 - \omega^2}, \end{aligned} \tag{32}$$

and

$$\begin{aligned} \lambda_{Z_s} &= \lambda + sk - i\omega k\beta, \\ s &= -\frac{k}{2} + i\omega\beta \pm \sqrt{\left(\frac{k}{2}\right)^2 - \omega^2}, \end{aligned} \tag{33}$$

and finally

$$\begin{aligned} \lambda_{Z_T} &= \lambda + sk - i\omega k\beta, \\ s &= -\frac{k}{2} + i\omega\beta \pm \sqrt{\left(\frac{k}{2}\right)^2 - \omega^2}. \end{aligned} \tag{34}$$

In the low-frequency limit $\omega \ll k$ we find that

$$\begin{aligned} &s \simeq -2k + i\omega\beta, \qquad s \simeq i\omega\beta - \frac{\omega^2}{2k}, \\ &s \simeq -k + i\omega\beta + \frac{\omega^2}{k}, \qquad s \simeq i\omega\beta - \frac{\omega^2}{k}, \end{aligned} \tag{35}$$

whereas in the high-frequency limit $k \ll \omega$, we have

$$s \simeq -k + i\omega(\beta \mp 1), \qquad s \simeq -\frac{k}{2} + i\omega(\beta \pm 1), \tag{36}$$

so at lower frequencies half of the modes are damped less. In the high-frequency limit, the damping scheme causes a exponential decay of the constraints with a decay rate of $-k$ and $-k/2$ respectively.

III. NUMERICAL RESULTS

In this section we present our numerical results. Spherical symmetry is assumed. We perform a detailed analysis of the damping scheme applied to the evolution of flat spacetime with different constraint-violating perturbations in order to reproduce the analytic results and explore the regime not accessible to a pen-and-paper analysis. We consider then nontrivial initial data composed of either punctures or a compact star and evolve them using different values for the damping parameters. In this case the performance of the damping scheme in a strong-field regime on constraint violations related, essentially, to different truncation errors are investigated. The code employed is described in detail in [10].

Numerical setup. In all numerical simluations we use fourth-order finite differences for the discretization of the spatial derivatives of the metric fields. For the time integration we use Runge-Kutta fourth order in the vacuum and puncture tests. In the simulation of the compact star we employ the Runge-Kutta third order in combination with a high-resolution shock capturing based on the local Lax-Friedrichs flux and the convex-essentially-non-oscillatory interpolation for the reconstruction of the matter fields. Table I summarizes the numerical settings employed for the results presented; convergence tests were run on some cases (see also discussions in the following paragraphs).

TABLE I. Setting used for the numerical simulations presented in this paper. The resolution is given in grid points, $r_{\rm out}$ is the coordinate location of the computational boundary, and $\alpha_{\rm CFL}$ is the Courant-Friedrichs-Levy factor used in the time-stepping.

Initial data	Resolution	$r_{\rm out}$	$\alpha_{\rm CFL}$
Flat	4000	100 a.u.	0.5
Puncture	1000	50 M	0.5
Star	2000	50 M	0.4

A. Perturbed flat spacetime experiments

Initial data and parameter space. Perturbations of flat spacetime are constructed, depending on which of the two eigenmodes, u_Θ, u_ω, we want to analyze, by modifying the χ variable to

$$\chi(0, r) = 1 + A \exp\left(-\frac{r^2}{2b^2}\right) \cos\left(\frac{2\pi\nu}{b} r\right), \tag{37}$$

or the $\tilde{\Gamma}^r$ variable,

$$\tilde{\Gamma}^r(0, r) = Ar \exp\left(-\frac{r^2}{2b^2}\right) \cos\left(\frac{2\pi\nu}{b} r\right). \tag{38}$$

Simulations employing the first kind of initial data are analyzed by looking at the eigenmode u_Θ, while those employing the second kind by looking at u_ω. The eigenmodes are Fourier-transformed in space for every time step, and their decay is studied by means of the power spectral density at the frequency $\tilde{\nu} = \frac{\nu}{b}$.

The parameter space, depicted in Fig. 1 (left panel), is spanned by the amplitude A and the frequency ν of the initial constraint violation. We vary also $\kappa_1 = k \in [0, 1]$ but keep for simplicity $\kappa_2 = 0$. The parameter $b = 10$ (fixed) introduces a length scale to the problem, which is useful for tuning the frequency ν (number of cycles in the period b, see right panel of Fig. 1). To evaluate the strength of the perturbation, the value of the perturbation's amplitude A should be compared with unity, see Eq. (37).

High-frequency, low-amplitude corner. In this region of the parameter space the analytical results hold. We set $\nu = 10$ ($\tilde{\nu} = 1$) and $A = 10^{-4}$, Fig. 2 display the results obtained. The numerical data show an exponential decay of the power spectral density at the induced frequency $\tilde{\nu}$ for both eigenmodes and for different values of the damping

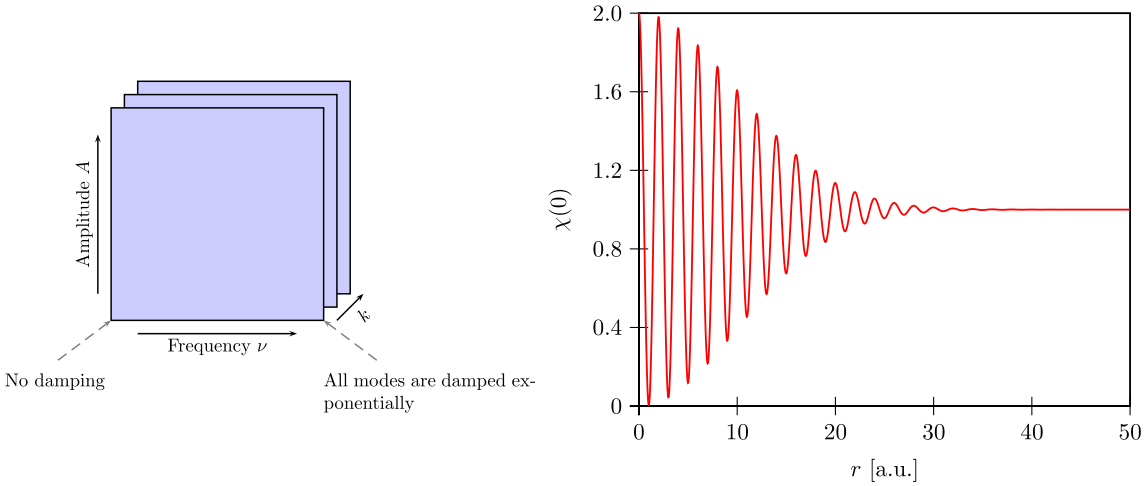

FIG. 1 (color online). (Left) Parameter space for the constraint violation of flat spacetime. The violation can be tuned by its amplitude A and frequency ν. Analytically known are the low-frequency corner, where the violation is not damped and the high-frequency, low-amplitude corner where all modes are damped exponentially. (Right) Shape of the constraint-violating initial data. A Gaussian curve with amplitude A and full-width half-maximum b is modulated with the frequency ν/b. The parameter ν tells how many oscillations are within b. The figure shows the constraint violation in χ at $t = 0$ with $A = 1$, $b = 10$ and $\nu = 5$.

parameter k. The rate is quantified by linear fitting as displayed in Fig. 3. Table II reports the decay rates for different values of k and different grid resolution (n is the number of grid points), together with the computed fitting error. Almost for every case the analytically predicted values, i.e. $s \approx k$ (for u_Θ) and $s = \frac{k}{2}$ (for u_ω), lie within the error range of the numerically found number. For increasing resolution the error gets smaller. Note that the large error is caused by the oscillations of the modes. The decay rates of the modes agree much better with the analytically predicted values than our conservative error estimate suggests (see Fig. 3).

From high to low frequency. To explore the low-frequency regime, we keep the low amplitude $A = 10^{-4}$ and vary the frequency in the range $\nu = [0, 10]$. Analytic results indicates that there is no damping for constant in space modes (zero-frequency modes). The numerical experiments show that, for decreasing values of the initial perturbation frequency in the range $[2, 10]$, the damping scheme remains effective with the analytic exponential decay rates. The behavior is displayed in Fig. 4.

The transition from exponential damping to no damping happens after the second octave $\nu \in [0, 2]$, Fig. 5. As demonstrated by the plot the transition is smooth and quite

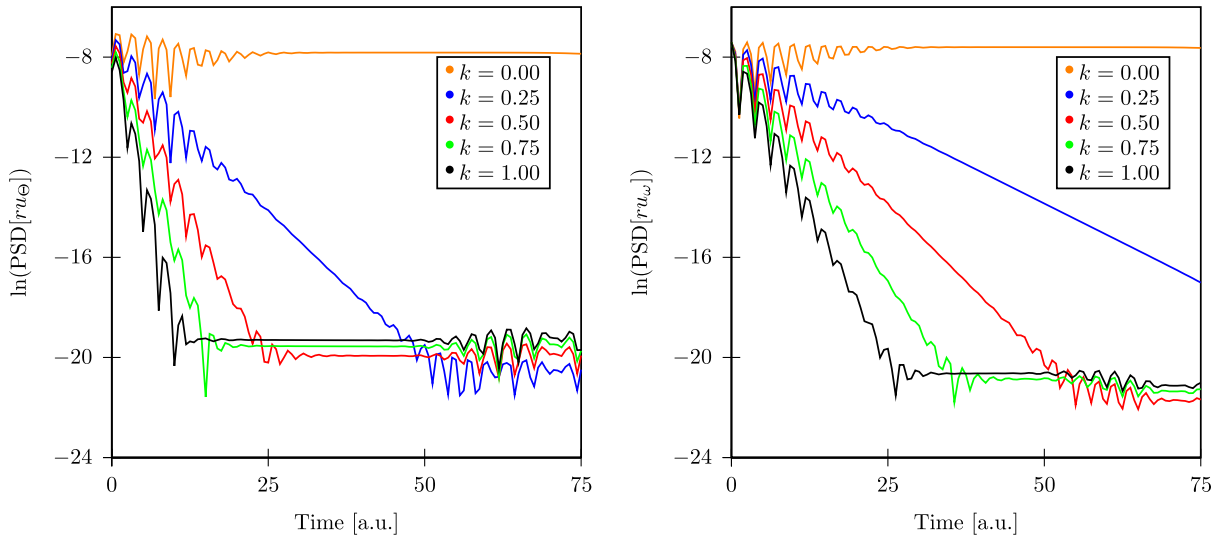

FIG. 2 (color online). Behavior of the eigenmodes u_Θ (left) and u_ω (right) for high-frequency $\nu = 10$, low-amplitude $A = 10^{-4}$ constraint violation. The modes are extracted in the Fourier space at $\bar{\nu} = 1$. For no damping ($k = 0$) the modes are stay constant. For a $k > 0$ the modes are damped exponentially with different damping rates.

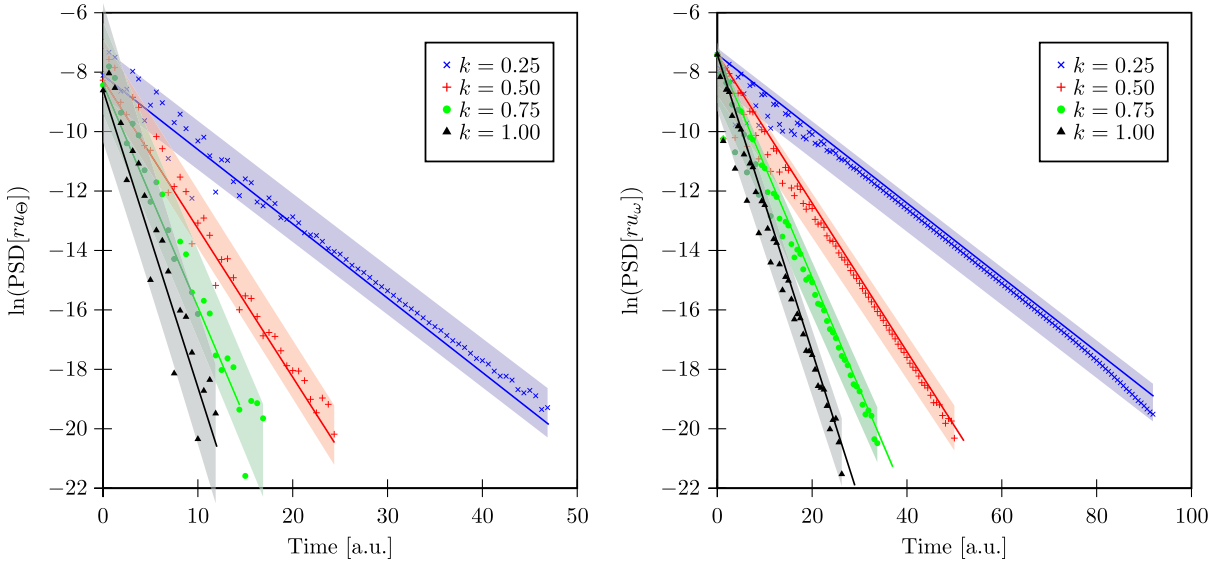

FIG. 3 (color online). Fit of the exponential decay of the eigenmodes u_Θ (left) and u_ω (right) for high-frequency $\nu = 10$ and low-amplitude $A = 10^{-4}$ constraint violation. The analytically predicted decay rates (solid lines) lie in every case within the 68% confidence interval of the fits which are represented in the figure by the shaded regions.

rapid. The experimental fact, observed here, that constraint-violating modes of "almost all" nonzero frequencies are killed by the damping scheme can be important in numerical relativity simulation.

From low to high amplitude. Increasing the amplitude of the perturbation, i.e. moving from a perturbative regime to a fully nonlinear situation is a delicate procedure. Our results can be summarized as follows.

High-amplitude perturbations, up to $A \simeq 0.1$, are damped and the damping rates unaffected. The use of progressively higher amplitudes first modifies the damping rates (constraint-violating modes are less damped) and secondly leads to unphysical results and code failures. The maximum amplitude which can be reached without changing the damping parameter k depends on the frequency of the initial perturbation. For low-frequency initial perturbations higher amplitudes are effectively damped by the damping scheme than for high frequencies.

TABLE II. Fits results for the decay rates for different resolutions. The parameters of the initial perturbation are $\nu = 10$ and $A = 10^{-4}$.

k	s ($n = 2000$)	s ($n = 4000$)	s ($n = 8000$)	s_{analytic}
0.25	-0.21 ± 0.02	-0.24 ± 0.02	-0.25 ± 0.01	-0.25
0.50	-0.49 ± 0.06	-0.51 ± 0.04	-0.50 ± 0.04	-0.50
0.75	-0.74 ± 0.09	-0.78 ± 0.08	-0.77 ± 0.05	-0.75
1.00	-0.93 ± 0.16	-1.02 ± 0.20	-1.02 ± 0.14	-1.00
0.25	-0.12 ± 0.01	-0.12 ± 0.01	-0.12 ± 0.01	-0.125
0.50	-0.24 ± 0.02	-0.24 ± 0.02	-0.24 ± 0.01	-0.250
0.75	-0.35 ± 0.04	-0.35 ± 0.04	-0.36 ± 0.02	-0.375
1.00	-0.47 ± 0.07	-0.48 ± 0.07	-0.48 ± 0.03	-0.500

Furthermore, it is not true that increasing k generically allows for higher amplitudes. The dependence on the damping parameter is not monotonic, the optimal value for this problem has been experimentally found to be $k = 0.5$.

Figure 6 shows that, for $k = 0.5$ and $\nu = 10$, the damping rates stay the same as in the low-amplitude case for an amplitude range $A \in [0.0001, 0.01]$. Setting the amplitude to $A = 0.1$, the damping is no longer exponential and, for higher values, the code gives no reasonable result.

Resolution dependency. Convergence of the results has been already reported in Table II and briefly discussed; we further comment here focusing on representative simulations with $k = 0.5$, $\nu = 10$, $A = 10^{-4}$ with varying resolutions. As shown in Fig. 7 the damping effect holds longer for higher resolutions, i.e. if the frequency of the constraint violation is better resolved, then the damping scheme works more effectively. This suggests that the damping scheme works as long as the frequency of the perturbation is well-resolved and it is partially expected since it acts at the continuum level. The same effect could have been already anticipated from Fig. 4, which refers to a single resolution but different frequencies which are resolved differently on the grid.

Very high frequencies, grid modes and dependency on artificial dissipation. The effect of the damping scheme on frequencies comparable to or of the order of the numerical grid (grid modes) is finally studied [19]. For these tests we use $k = 0.5$ and vary the frequency $\nu \in [10, 30]$ (Note the grid spacing is $h = 0.025$.). As demonstrated in Fig. 8, if the frequency ν of the perturbation is increased further to a regime where the signal is not well-resolved, the damping becomes progressively less effective and deviates from the

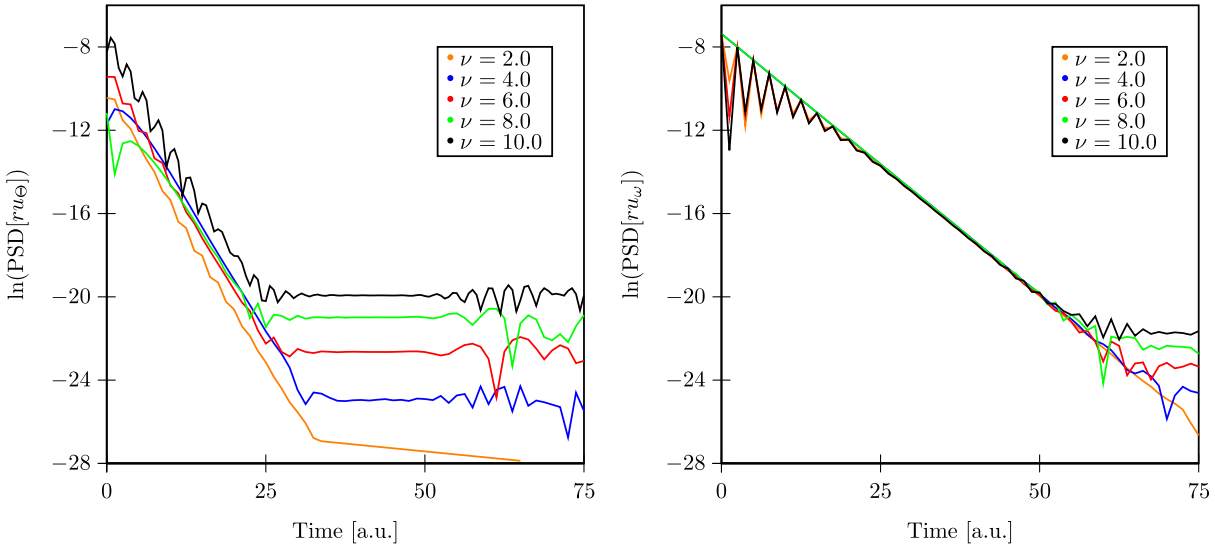

FIG. 4 (color online). The rate of the exponential decay of the eigenmodes u_Θ (left) and u_ω (right) for low-amplitude $A = 10^{-4}$ constraint violations stays constant in the frequency range $\nu \in [2, 10]$.

analytic expectation. More importantly, the amount of artificial dissipation [20] plays a significant role. The use of the artificial dissipation filters out grid modes and generically attenuates high frequencies which are aliased to lower ones. Figure 9 (left panel) shows that the use of different amounts of dissipation, σ, quantitatively changes the decay rate of the eigenmodes. The higher σ is, the higher the damping rate. However one cannot expect to use arbitrary large values of σ, so a balance between k and σ and the property of the solution have to be studied case by case by performing convergence tests. In our test case we found that $\sigma = 0.05$ roughly reproduce the analytic damping rates.

As a final test we evolve initial data containing random noise,

$$\chi(0, r) = 1 + A \exp\left(-\frac{r^2}{2b^2}\right) \mathrm{rand}([-1, 1]). \tag{39}$$

Note that, in principle, random noise differs from the high-frequency perturbation used before because it has a flat spectrum. Figure 9 (right panel) shows that the effectiveness of the damping scheme depends again strongly on the value of σ in the artificial dissipation operator used. However, differently from the previous case, in this case we were not able to recover the analytic damping rates.

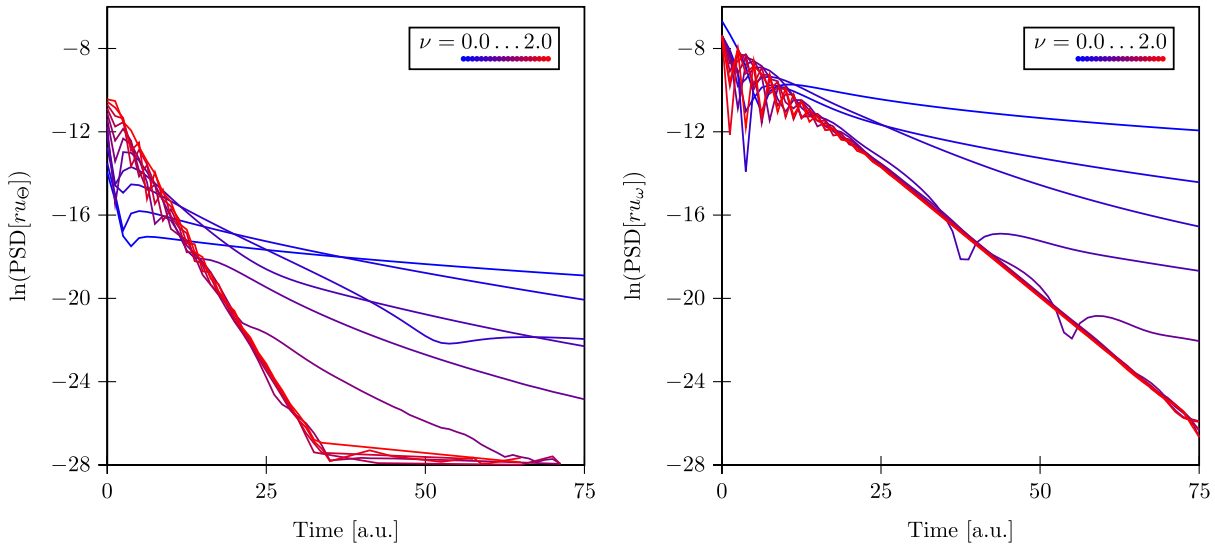

FIG. 5 (color online). In the small-frequency range $\nu \in [0, 2]$ the transition between exponential damping and no damping happens. The figure shows for low-amplitude $A = 10^{-4}$ constraint violations the decay of the eigenmodes u_Θ (left) and u_ω (right).

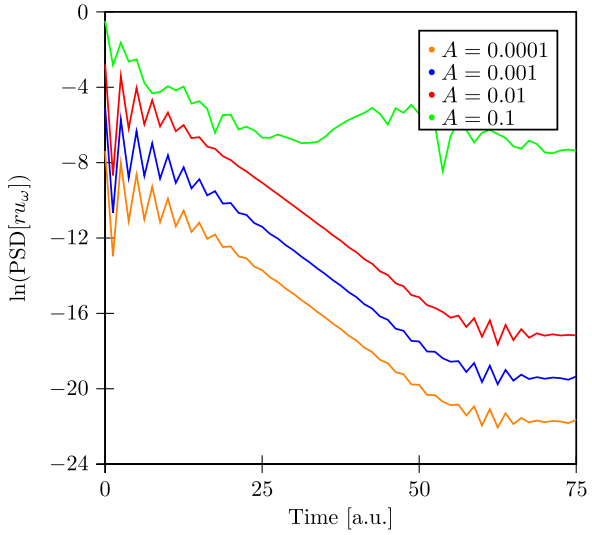

FIG. 6 (color online). Decay of the eigenmode u_ω for high-frequency constraint violation with increasing amplitude A. Between $A = 10^{-4}$ and $A = 10^{-2}$ the damping rate does not change. For very high-amplitude $A = 10^{-1}$ the damping of the eigenmode is not exponential anymore and the code does not give physically reasonable results.

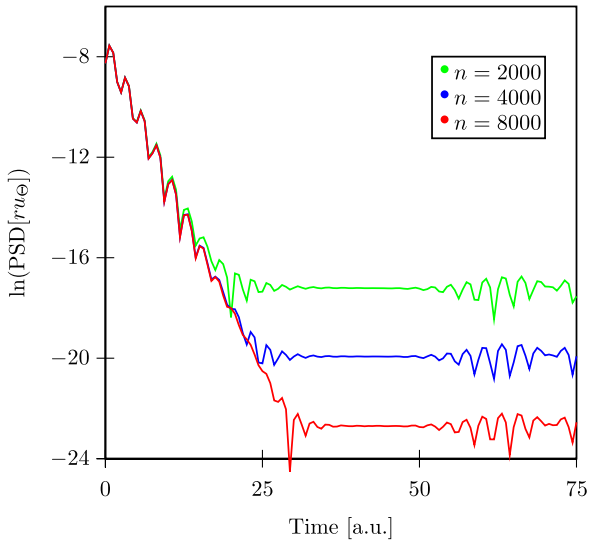

FIG. 7 (color online). The damping effect depends on the resolution of the initial constraint violation. The figure shows for high-frequency $\nu = 10$, low-amplitude $A = 10^{-4}$ the damping of the eigenmode u_Θ for different resolutions. For high resolution the frequency is well-resolved and therefore the damping effects lasts longer than for less well-resolved case.

B. Punctures and compact star experiments

Single puncture. In order to test the damping effect on strong-field evolution, we evolve puncture initial data [21]. While the initial data are constraint-satisfying, a constraint-violating wave leaving the hole and propagating outside is observed in numerical simulations. This feature

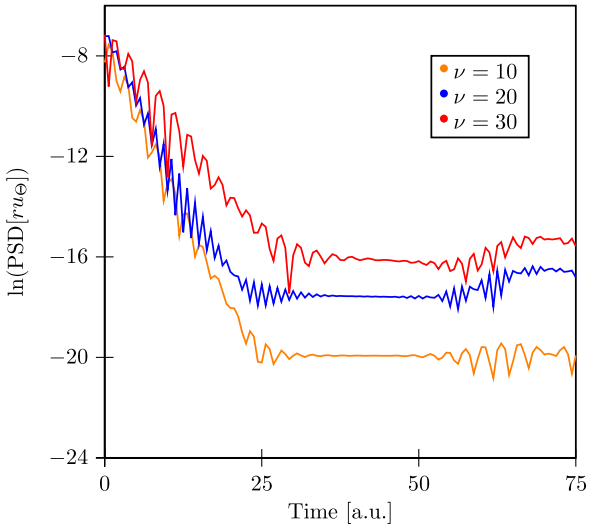

FIG. 8 (color online). Increasing the frequency of the initial constraint violation with low-amplitude $A = 10^{-4}$ even further to very high frequencies. At these high frequencies the constraint violation get less resolved which weakens the effect of the damping.

is generic and not related to the use of Z4, but observed also in BSSNOK evolutions, e.g. [22]. Note however that the constraint violation is converging away with resolution, thus not a continuum feature (the constraint subsystem in Z4c does not have superluminal speeds). Figure 10 (left panel) shows a snapshot of the constraint violation leaving the horizon. During the evolution the biggest violation is instead found at the puncture, where the solution is not smooth. *A priori*, the frequency of the initial constraint-violating wave, as well as the later violation at the puncture, cannot be estimated, whereas their amplitude is expected to be "small" (in the sense that it is converging away). From Fig. 10 it is evident that the frequency of the constraint-violating wave spans a certain range of frequencies; in terms of the length scale given by the mass, $M = 1$, we mainly observed violation at a peak frequency $\bar{\nu} \sim 0.5$. It can be considered a high and we expect it to be damped since it is within the first octave.

The numerical evolutions performed with different values of k show that the use of the damping scheme generically introduces a certain dynamics in the constraints, whose values in space oscillates in time around a small value close to zero. The evolution of the L2 norm of the constraint monitor

$$C = \sqrt{H^2 + M^i M_i + \Theta^2 + Z^i Z_i} \tag{40}$$

is reported in Fig. 11 (left panels) for different values of k. In these tests artificial dissipation is used with $\sigma = 0.007$. In all the cases the norm at early times is dominated by a violation inside the horizon during the gauge adjustment which leads to the trumpet solution [23–28]. The initial constraint violation wave is also propagated out during this

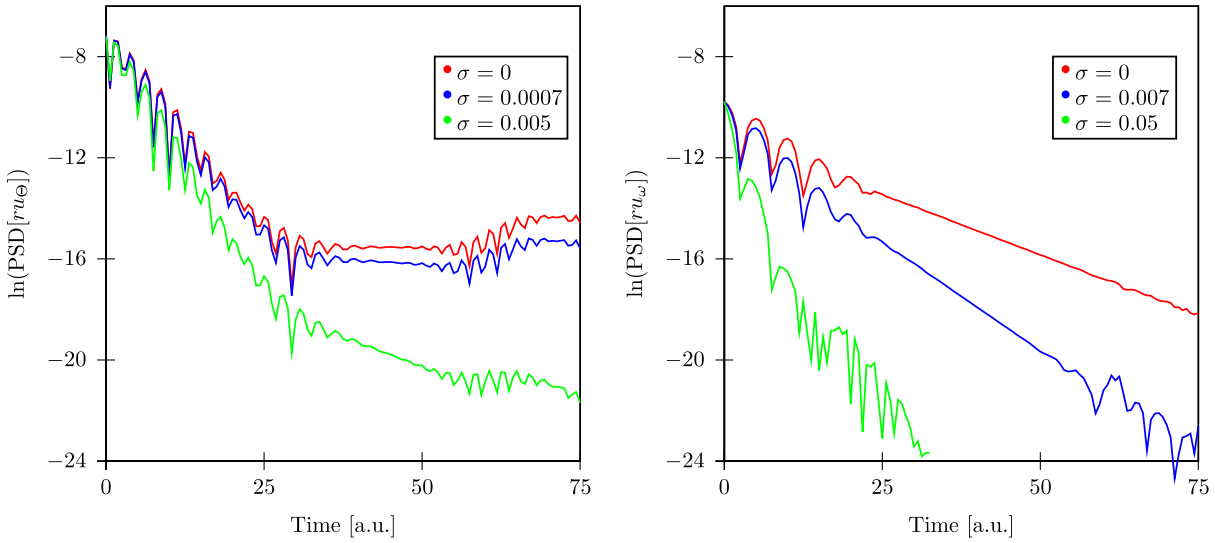

FIG. 9 (color online). For initial constraint violations with low amplitude and very high frequency, the artificial dissipation starts to have an effect. The high-frequency modes are shifted by the artificial dissipation to lower frequencies which are then damped. The figure shows the dependence of the decay of the eigenmode u_Θ on the artificial dissipation parameter σ using high-frequency $\nu = 30$ (left) and random noise constraint violation initial data (right).

phase, and eventually damped depending on the value of k. The bottom left panel shows the norm outside the horizon at early times and highlights the effect of the damping scheme for several values of k. At later times the amplitude of the oscillations in the constraints amplifies around $t \sim 1.25 \times 10^3\ M$ as shown in the top left panel. Depending on the value of k, the amplification is observed to saturate and damp ($k < 0.2$) or to keep on growing, contaminating the numerical solution ($k > 0.2$). In the latter case the code eventually fails because the boundary conditions implemented [11] can not sustain such a large violation.

To assess the relative importance of boundary conditions and the constraint damping scheme in our numerical experiments, we performed long evolutions of a single puncture with and without both the damping scheme, and either constraint-preserving [11] or Sommerfeld boundary conditions. The outer boundary was placed at 50 M. The results are presented in Fig. 12. We find that the use of constraint-preserving boundary conditions is more important than that of the damping scheme in avoiding violations. Although the use of the damping scheme with $k = 0.02$ reduces the violation by a factor of 9 when Sommerfeld conditions are used. This test is not expected to be representative of more general scenarios in which the outer boundary is placed farther out with the same resolution, since then, experimentally we find that a smaller constraint violation interacting with the Sommerfeld condition results in smaller reflections. On the other hand,

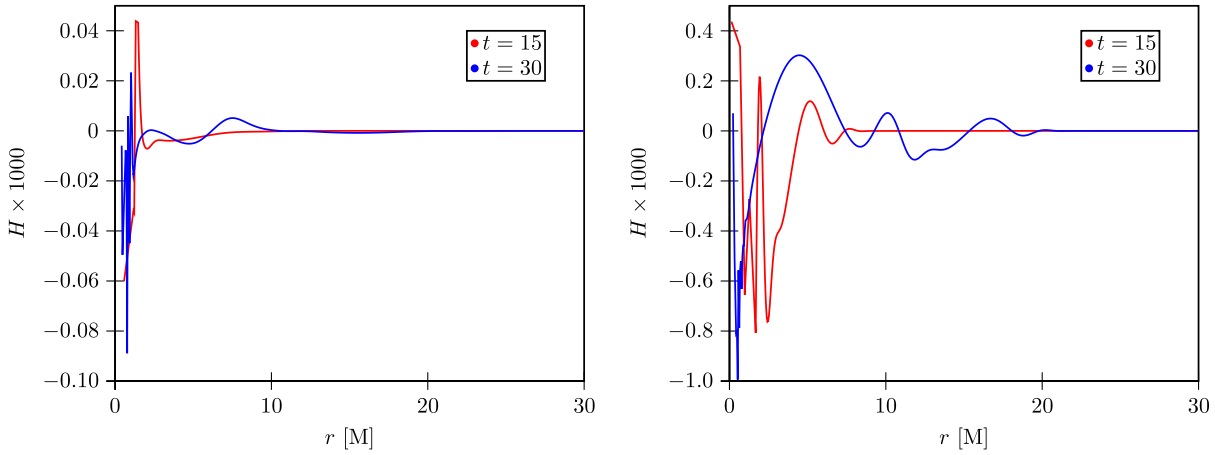

FIG. 10 (color online). The puncture and the stuffed puncture initial data violate the constraints. This constraint violations leave the black hole horizon. The figure shows the Hamiltonian constraint H at time $t = 15\ M$ and $t = 30\ M$. (Left) Puncture initial data, (right) Stuffed puncture initial data.

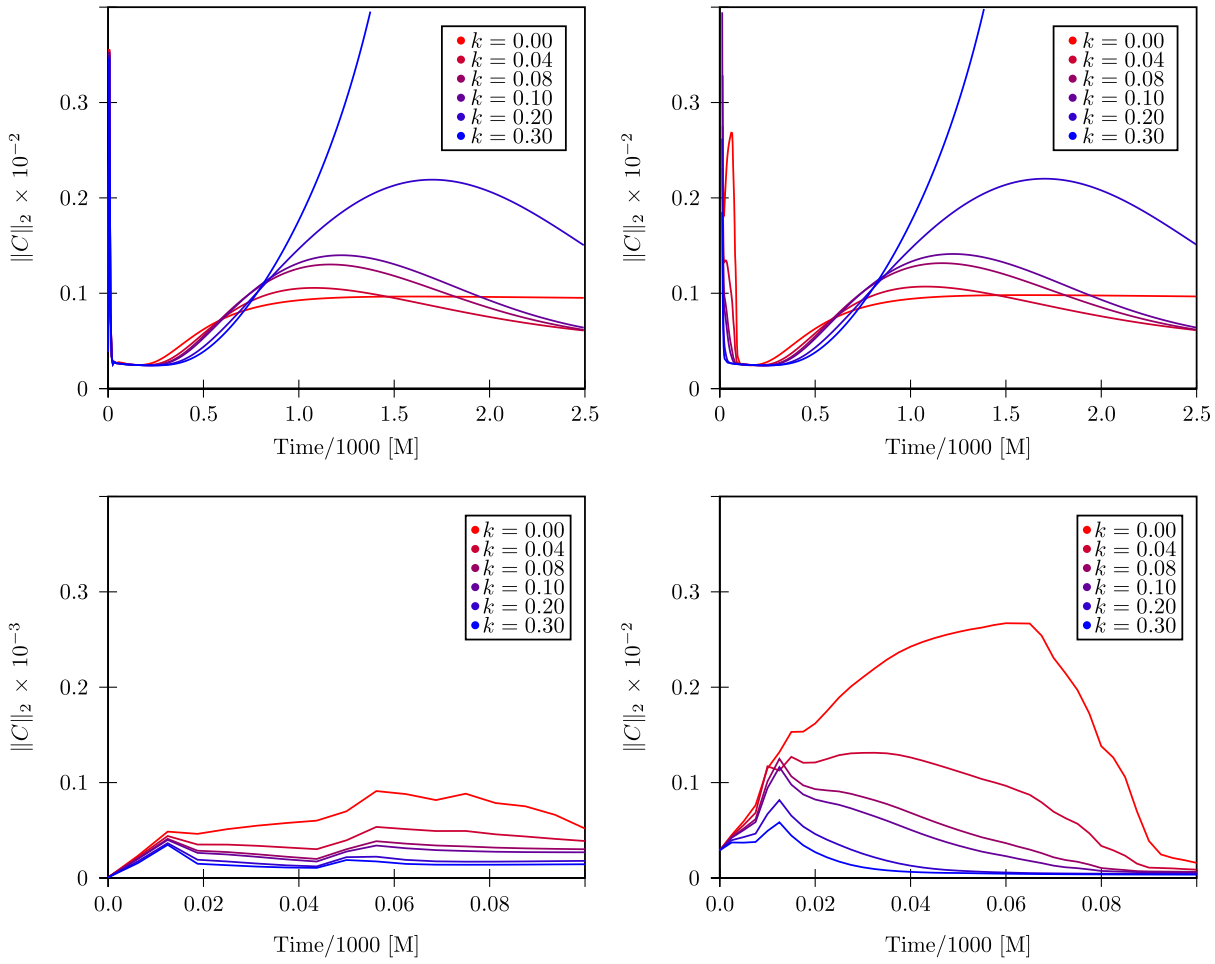

FIG. 11 (color online). Time evolution of the norm of the constraint monitor. For the figures on the left puncture initial data was used, for the figures on the right stuffed puncture initial data. The long time behavior of both cases is the same which can be seen in the pictures on the top. The difference between the two initial data can be seen in the two figures on the bottom which show the norm of the constraint monitor outside the horizon for early time. The stuffing introduces a big constraint violation compared to the normal puncture data. This violation is damped away. The longtime behavior depends on the value of the damping parameter while for damping parameter $k < 0.3$ the damping scheme does not cause problems in the evolution, damping parameter $k \geq 0.3$ introduce dynamics to the system which leads to increasing constraint violation and a crash of the code.

since the constraint-preserving conditions are found to converge numerically, and the Sommerfeld conditions do not, it is expected that at some resolution the constraint violation induced by the Sommerfeld conditions will become dominant, even if the outer boundary is placed far out. This has been recently pointed out for the case of 3d matter simulations and of BSSNOK in [29].

Stuffed puncture. A second series of tests performed is the evolution of puncture initial data stuffed in the black-hole interior [22,30,31]. The hole has been stuffed inside the horizon $r_h = M/2$ at $r_{\rm ex} = 0.475$ using a fourth-order polynomial in the conformal factor

$$\psi(0, r) = 2.97368 - 5.83175\left(\frac{r}{M}\right)^2 + 7.75413\left(\frac{r}{M}\right)^4. \tag{42}$$

The polynomial matches the puncture data at $r_{\rm ex}$ up to the second derivatives. The initial data are clearly constraint-violating and also show the outgoing constraint-violation wave Fig. 10 (right panel). The evolution of the constraint monitor for different k is reported in the right panels of Fig. 11. Only quantitative differences with respect to the puncture case are observed. As demonstrated in the right bottom panel of Fig. 11 (note the difference in the scale with respect the left panel), the damping scheme is again effective in reducing the outgoing constraint violation during the initial adjustment. At late times the situation is completely analogous to the puncture evolution and we do not repeat the description, see top right panel.

Stable star. As a final test, we present a study of the influence of the damping scheme on the evolution of a stable equilibrium model of a compact star of mass

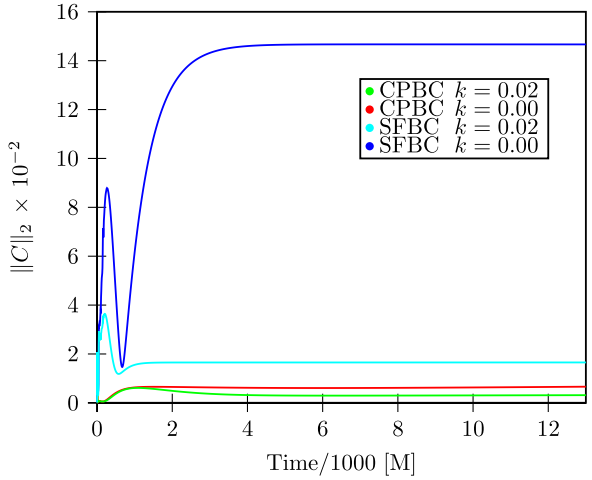

FIG. 12 (color online). Long-term evolution of a puncture with the Z4c formulation. Different boundary conditions were tested with and without damping (with $k = 0.02$). Sommerfeld boundary conditions lead to a high constraint violation, which is effectively suppressed by the damping scheme. Using Sommerfeld, the constraint violation is roughly a factor of 9 lower with and without damping at late times. Using constraint-preserving boundary conditions, without damping, leads to a late-term constraint violation which is 20 times lower than that of undamped Sommerfeld. The damping is less important in the case of constraint-preserving boundary conditions. Using the standard damping value $k = 0.02$, the improvement is by only a factor of 2.

$M = 1.4\ M_\odot$ described by the ideal gas equation of state. Initial data are the same as those employed in previous works [10,11] and constraint-satisfying. Furthermore they provide the exact solution for the evolution problem since the system is static. At the typical resolutions employed (and without damping, $k = 0$) stable evolutions are obtained for about 10 ms ($t \sim 1400\ M$). Truncation errors trigger radial oscillation in the star, which are small amplitude, low frequency in space constraint-violating modes, $\nu \sim 1/(2R)$ where R is the star coordinate radius.

In previous investigations on stable stars, which considered only one value of the damping parameter, we found that the constraint damping terms have a negligible effect on the dynamics, while constraint propagation made a large difference with the equivalent BSSNOK simulations [10]. The new results discussed here confirm the previous ones for the specific k considered, but they also show that for certain values of the damping parameter the constraint damping terms are not beneficial in the long-term evolutions.

Figure 13 shows the evolution of the central rest-mass density (left) and of the L2 norm of the constraint monitor (right) for different values of k employed in the damping scheme. For $k \geq 0.3$ the constraint damping amplifies the radial oscillations and drives the star to collapse. Large constraint violations indicate the departure from the constraint-satisfying solution space (for clarity they are not shown in the right panel). Smaller values of $k \leq 0.06$ produce instead an effective constraint damping at early times (see right panel Fig. 13). In the long term however, the evolution without damping scheme ($k = 0$) is always preferable to the evolutions with $k \geq 0.03$. In the latter cases a long-term growth is observed, similar to that seen in the puncture simulations. The value $k = 0.02$ leads to a constraint-damped evolution, but its effect is almost negligible. More importantly, this choice is not robust in other tests performed. In both simulations employing a different equation of state, specifically a polytrope which produces different truncation errors at the surface of the star, and in

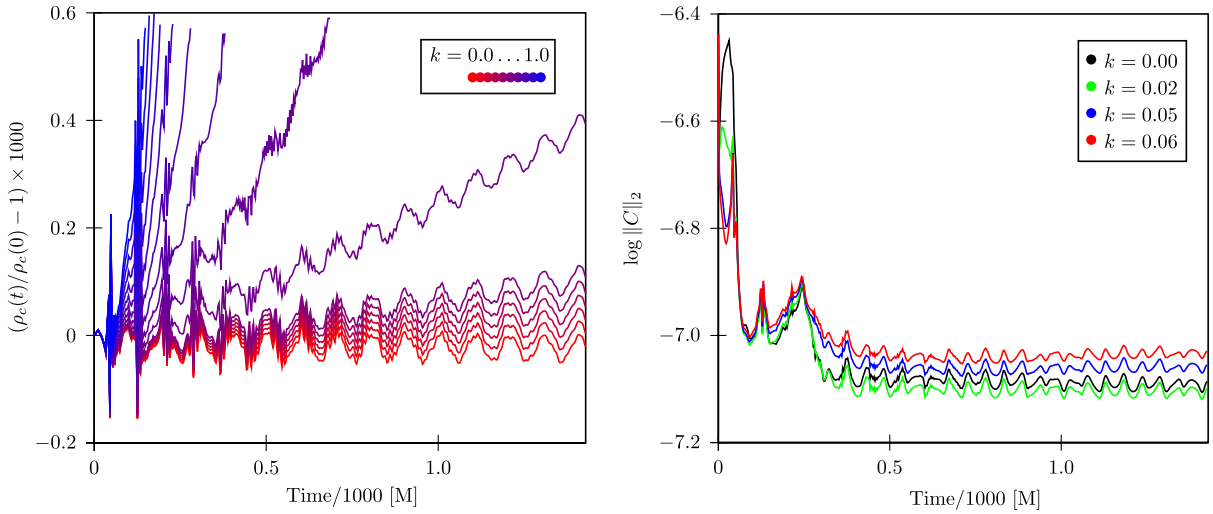

FIG. 13 (color online). (Left) Time evolution of central rest-mass density for a stable star obtained using different values of k. (Right) Time evolution of the constraint monitor corresponding to a subset of the evolutions of the right panel.

the migration test of [10] we were not able to identify a value of k which leads to an efficient constraint damping. We presented here in detail only the test with the most varied outcome.

While the static stable star is a delicate test (every small perturbation causes a departure from the Einstein solution), it provides a specific relevant example in which the constraint damping fails for a large choice of damping parameters. This indicates that the use of the constraint damping scheme without specific investigations is potentially dangerous.

IV. CONCLUSION

In order to expand the body of evidence that a conformal decomposition of the Z4 formulation of general relativity [2] may be a useful tool for numerical relativity we have presented a detailed study of the effect of the constraint damping scheme of Gundlach *et al.* [8].

We have attempted to answer three questions, which we address here specifically:

(i) *Under what conditions can the theoretically predicted damping rates be recovered in the numerical approximation?* By studying the evolution of parametrized constraint-violating perturbations on top of flat space, we first found that the predicted damping rates of [8] are recovered for well-resolved high-frequency constraint violations. Varying the frequency of the constraint violation, we found that the analytically predicted exponential decay is maintained over a large, three-octave, range. The cutoff in the effectiveness of the scheme occurs over a small range at low frequencies. On grid noise, unsurprisingly, we find that the predicted damping rates are not recovered, although the combination of damping and artificial dissipation does help to suppress constraint violations. The intuitive explanation for this is that artificial dissipation aliases the grid noise to lower frequencies which are well-resolved, and on which the damping scheme is effective. Finally we increased the amplitude of the constraint violation. At amplitudes above $A \simeq 0.1$ the damping scheme becomes increasingly less effective, after which numerical integration is often not possible, either with or without constraint damping.

(ii) *How effective is the damping scheme in astrophysically relevant spacetimes?* For this part of the investigation we began by evolving a single puncture black hole. We find that the constraint damping scheme suppresses constraint-violating numerical error leaving the black hole horizon, but that it generically introduces a dynamical behavior to the constraints. The suppression of the violation leaving the horizon is furthermore not dramatic. For reasonable values of the damping parameter a factor of about 2 or 3 is gained in the norm of the constraint violation. If the damping parameters are chosen too large, the dynamical behavior induced by the scheme causes a large constraint violation to hit the outer boundary, which in our tests was placed at 50 M, eventually causing a code failure, which we think it may be possible to avoid by including constraint damping terms in the constraint-preserving boundary conditions [11] appropriately. Since mixed puncture black-hole-neutron-star initial data are not readily available, ''black-hole stuffing'' has been proposed [22,30,31]. Therefore to investigate the likely effect of the constraint damping scheme in mixed binary evolutions, we evolved a single puncture with a constraint-violating interior. Here we find qualitatively the same behavior as in the single puncture evolutions, the only difference being that the size of the constraint-violating numerical error leaving the black hole is larger. Finally on the question of astrophysically relevant spacetimes evolutions of a static star were performed. Here we find that using the damping scheme is generically of minor benefit and can cause an unphysical collapse.

(iii) *In practical applications what are reasonable values for the constraint damping coefficients?* Our flat-space tests demonstrate that higher values of the damping parameters are preferable, because then faster rates of exponential damping are achieved. On the other hand, since our evolutions of compact objects suffer from severe problems when the damping parameters are chosen too large, we suggest that the damping parameter are chosen in the range $k \in [0, 0.1]$ for puncture evolutions while for matter evolution the safest option to use $k = 0$ unless specific damping tests are performed.

In summary, at least for the spherical symmetric systems studied within this work, the following statements about the constraint damping scheme can be made: Considering vacuum spacetimes, the damping scheme may be, for carefully chosen damping parameters, a useful tool for suppressing constraint violations. This is certainly true if there are features in the numerical setup which cause large constraint violations, for example, Sommerfeld boundary conditions or constraint-violating initial data. If no such features are present, the damping scheme is not essential and can furthermore affect the physics of the system if the damping parameters are taken too large. In the evolution of a static compact star our numerical evidence indicates that the damping scheme sometimes leads to a slight decrease of constraint violation. On the other hand the damping scheme, in combination with some numerical setups, causes growth of the constraints; in the special cases we have considered the damping scheme is of marginal use.

ACKNOWLEDGMENTS

The authors would like to thank Bernd Brügmann and Milton Ruiz for helpful discussions. We also thank the authors of [14] for valuable comments on the manuscript, and, in particular, Carlos Palenzuela for his query on our neutron star results. This work was supported in part by DFG grant SFB/Transregio 7 ''Gravitational Wave Astronomy,'' the DLR grant LISA Germany, and the DFG Research Training Group 1523/1, ''Quantum and Gravitational Fields.''

[1] Othmar Brodbeck, Simonetta Frittelli, Peter Hubner, and Oscar A. Reula, J. Math. Phys. (N.Y.) **40**, 909 (1999).
[2] C. Bona, T. Ledvinka, C. Palenzuela, and M. Zacek, Phys. Rev. D **67**, 104005 (2003).
[3] C. Bona and C. Palenzuela, Phys. Rev. D **69**, 104003 (2004).
[4] C. Bona, T. Ledvinka, C. Palenzuela, and M. Zacek, Phys. Rev. D **69**, 064036 (2004).
[5] C. Bona, T. Ledvinka, C. Palenzuela-Luque, and M. Zacek, Classical Quantum Gravity **22**, 2615 (2005).
[6] C. Bona and C. Bona-Casas, J. Phys. Conf. Ser. **229**, 012022 (2010).
[7] C. Bona and C. Bona-Casas, Phys. Rev. D **82**, 064008 (2010).
[8] Carsten Gundlach, Jose M. Martin-Garcia, Gioel Calabrese, and Ian Hinder, Classical Quantum Gravity **22**, 3767 (2005).
[9] Frans Pretorius, Phys. Rev. Lett. **95**, 121101 (2005).
[10] Sebastiano Bernuzzi and David Hilditch, Phys. Rev. D **81**, 084003 (2010).
[11] Milton Ruiz, David Hilditch, and Sebastiano Bernuzzi, Phys. Rev. D **83**, 024025 (2011).
[12] Manuela Campanelli, C. O. Lousto, P. Marronetti, and Y. Zlochower, Phys. Rev. Lett. **96**, 111101 (2006).
[13] John G. Baker, Joan Centrella, Dae-Il Choi, Michael Koppitz, and James van Meter, Phys. Rev. Lett. **96**, 111102 (2006).
[14] Daniela Alic, Carles Bona-Casas, Carles Bona, Luciano Rezzolla, and Carlos Palenzuela, arXiv:1106.2254.
[15] Carles Bona, Joan Masso, Edward Seidel, and Joan Stela, Phys. Rev. Lett. **75**, 600 (1995).
[16] Miguel Alcubierre *et al.*, Phys. Rev. D **67**, 084023 (2003).
[17] Helmut Friedrich, Classical Quantum Gravity **22**, L77 (2005).
[18] Milton Ruiz, Oliver Rinne, and Olivier Sarbach, Classical Quantum Gravity **24**, 6349 (2007).
[19] We use now the term high not related to the scale $\bar{\nu} \gtrsim 1$ of the continuum problem, i.e. not for $\nu \sim b$, but related to the characteristic frequency introduced by the numerical grid, i.e. $\nu \sim 1/h$.
[20] B. Gustafsson, H. O. Kreiss, and J. Oliger, *Time dependent problems and difference methods* (Wiley, New York, 1995).
[21] Steven Brandt and Bernd Bruegmann, Phys. Rev. Lett. **78**, 3606 (1997).
[22] J. David Brown, Peter Diener, Olivier Sarbach, Erik Schnetter, and Manuel Tiglio, Phys. Rev. D **79**, 044023 (2009).
[23] Mark Hannam, Sascha Husa, Denis Pollney, Bernd Bruegmann, and Niall O'Murchadha, Phys. Rev. Lett. **99**, 241102 (2007).
[24] Mark Hannam, Sascha Husa, Frank Ohme, Bernd Bruegmann, and Niall O'Murchadha, Phys. Rev. D **78**, 064020 (2008).
[25] David Garfinkle, Carsten Gundlach, and David Hilditch, Classical Quantum Gravity **25**, 075007 (2008).
[26] J. David Brown, Phys. Rev. D **77**, 044018 (2008).
[27] J. David Brown, Classical Quantum Gravity **25**, 205004 (2008).
[28] Marcus Thierfelder, Sebastiano Bernuzzi, David Hilditch, Bernd Brugmann, and Luciano Rezzolla, Phys. Rev. D **83**, 064022 (2011).
[29] Marcus Thierfelder, Sebastiano Bernuzzi, and Bernd Bruegmann, Phys. Rev. D **84**, 044012 (2011).
[30] Joshua A. Faber, Thomas W. Baumgarte, Zachariah B. Etienne, Stuart L. Shapiro, and Keisuke Taniguchi, Phys. Rev. D **76**, 104021 (2007).
[31] J. David Brown *et al.*, Phys. Rev. D **76**, 081503 (2007).